Elastic dipole theory of $CsCuCl_3$ and related hexagonal Jahn-Teller compounds for neutron scattering

1989 J. Phys.: Condens. Matter 1 3765

(http://iopscience.iop.org/0953-8984/1/24/002)

J. Phys.: Condens. Matter **1** (1989) 3765–3787. Printed in the UK

Elastic dipole theory of $CsCuCl_3$ and related hexagonal Jahn–Teller compounds for neutron scattering

U Schotte, H A Graf and H Dachs

Hahn-Meitner-Institut, Glienicker Strasse 100, D-1000 Berlin 39, Federal Republic of Germany

Received 27 June 1988, in final form 22 September 1988

Abstract. Yamada's proposal of treating as 'dense Huang scattering' the diffuse quasi-elastic intensities found in systems with distortive centres (=elastic dipoles) in each lattice cell is extended to a group of hexagonal cooperative Jahn–Teller compounds, with new experimental results available for one of them, $CsCuCl_3$. This proposal is put on firm ground by identifying 'dense Huang scattering' as the central component of the q- and ω-dependent neutron scattering cross section, which is calculated for the elastic dipoles in their elastic medium in terms of the three acoustic modes coupled to relaxing pseudo-spins. Phonon softening and the sign and size of strain-induced dipole interactions for possible ground-state structures are calculated.

1. Introduction

This paper continues an alternative description of the cooperative Jahn–Teller (JT) effect in hexagonal compounds $ABCl_3$ with A = Rb, Cs and B = Cu, Cr which are insulators and show one or two structural phase transitions from a common high-temperature (HT), high-symmetry phase $P6_3/mmc$ (figure 1). Of the extensive literature we point out recent work with review character and as a source for earlier work (Crama 1980, Crama and Maaskant 1983, Tanaka *et al* 1986a, b).

Recent quasi-elastic diffuse neutron scattering results for the HT phase of $CsCuCl_3$ (Graf *et al* 1986) revealed patterns typical for Huang scattering of impurities in an elastic medium. This led to the concept of an array of randomly oriented elastic dipoles localised at the Cu^{2+} or Cr^{2+} sites where the Jahn–Teller effect causes stretching or compression of the octahedral Cl^- cages around the Jahn–Teller ions, an idea introduced earlier by Yamada and co-workers (Mori *et al* 1980).

In contrast to Huang scattering from impurities—like interstitials or vacancies produced by irradiation—the distortions here are small compared to the lattice constants but the product of distortion times concentration is sizable. This explains why the q-range of validity of the Huang approach extends far in the Brillouin zone, and why the scattering disappears at T_c—or, rather, becomes unmeasurably small, although a few 'misfits' or domain boundaries should still be present at $T < T_c$. Also there are no problems with using the elastic constants as available. At T_c the elastic dipoles get ordered such that they tend to be parallel in the hexagonal plane and antiferrodistortively arranged along the c axis; for the Rb compounds there exist intermediate 'β-phases'.

0953-8984/89/243765 + 24 $02.50

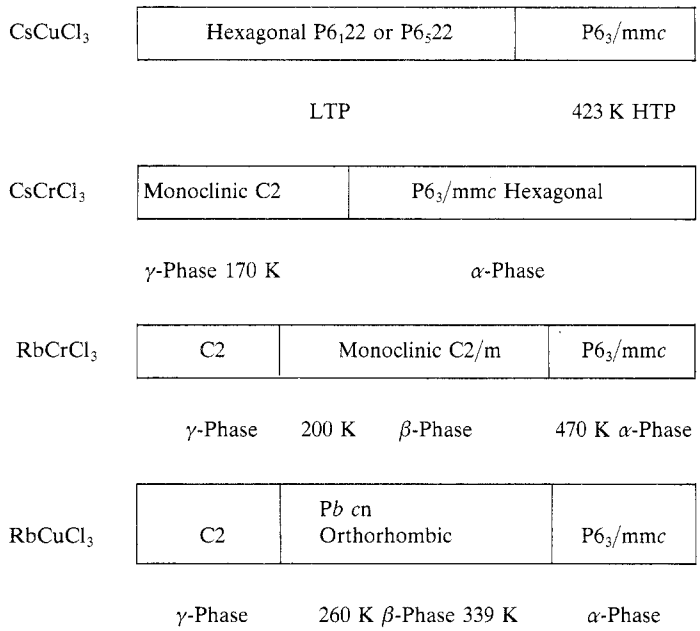

Figure 1. Structure and phase transition temperatures of the hexagonal JT compounds under investigation.

At low temperatures one finds stretched octahedra, and 'antiferrodistortive' means that the long axes never meet at the same anion. Since each octahedron has three axes which can stretch, one can map it on a three-state Potts spin (Schröder and Thomas 1976, Höck *et al* 1978) and several low-temperature structures are possible and indeed found. Rather unique is $CsCuCl_3$ in that the stretched axes are arranged in helices wound around the *c* axis (figures 2 and 3).

Most experiments have been performed on $CsCuCl_3$—the only compound where large single crystals of 'neutron quality' can be drawn from solution and the only

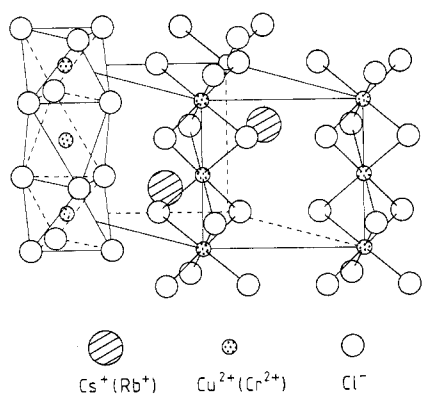

Figure 2. Parent structure ($CsNiCl_3$) of the hexagonal JT compounds.

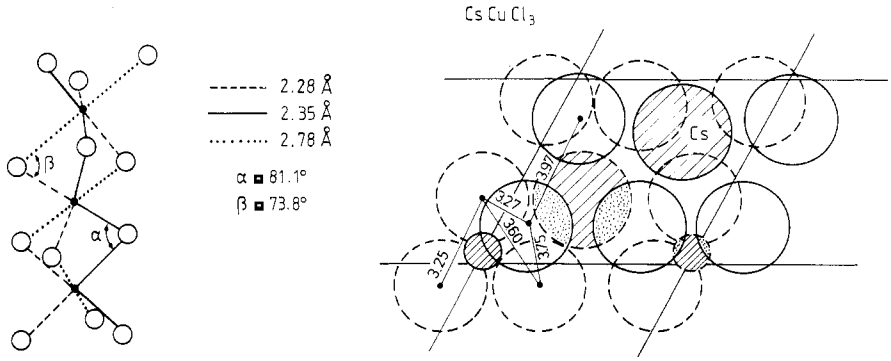

Figure 3. Structural details of $CsCuCl_3$ at room temperature: $CuCl_3^-$ chain determined by x-ray crystallography (space group $P6_122$).

one where room-temperature ultrasound results for the elastic constants are available (Soboleva *et al* 1976) and where temperature-dependent measurements of c_{44} show strong softening above T_c (Lüthi 1977). Therefore we test the theory on the results for $CsCuCl_3$.

In an earlier paper the above concept was elaborated and Huang scattering patterns calculated within a static picture of elastic dipole arrangements (Schotte 1987). To account for inelastic experiments and softening of acoustic waves, i.e. effects with $q \simeq 0$, the elastic approach can again be adopted, but must now include some dynamics; the experimental results point to a relaxation rather than to a resonance process. The theory will be developed such that the pseudo-spin relaxation rate is a fitting parameter, since this approach cannot describe the probably thermally activated hopping over a barrier of about 400 cm^{-1} separating the stretched octahedron states ('warping energy' of single JT complex).

The theory results in a more sophisticated treatment of 'dense Huang scattering', its temperature dependence and that of elastic constants involved in 'softening' of acoustic waves. The neutron scattering results available are well described. In addition, from strain-mediated dipole–dipole interactions, low-temperature structures can be anticipated. The system turns out to be describable by a very anisotropic three-state Potts model on two sublattices. We stress that we are not dealing with the first-order phase transition of $CsCuCl_3$ characterised by a tripling of the unit cell along the c axis. It is however suggested that no other dipole interactions are necessary to explain the observed dynamic and quasi-elastic phenomena.

2. The energy of the elastic dipoles in terms of acoustic phonons

With regard to their influence on the environment, the distorted octahedra can be replaced by elastic dipoles at their centres in one of six crystallographically possible orientations, as one can visualise with the help of figure 4. We divide them into two sublattices, one consisting of the lower type octahedra (distortive types $r = 1, 2, 3$) and the other of the upper type ($r + 3 = 4, 5, 6$).

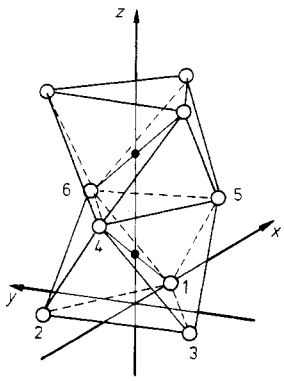

Figure 4. Double octahedron of the unit cell. The distorted octahedron is supposed to have the same principal axes as the mean undistorted octahedron (Schotte 1987). The numbers refer to tetragonal elongations, for example distortion 1 means that the axis from point 1 upwards is stretched,

Their pseudo-spin character or orientation is described by the variable $c^r(\boldsymbol{R}) = 1$ or 0, depending on whether distortive type r is present in site $\boldsymbol{R}$ or not. Usually one prefers the concentration fluctuation

$$c^r(\boldsymbol{R}) - \langle c^r(\boldsymbol{R})\rangle = c^r(\boldsymbol{R}) - c^r \tag{1}$$

which is also the order parameter with the properties

$$\sum_r [c^r(\boldsymbol{R}) - c^r] = 0$$

$$\langle c^r(\boldsymbol{R}) - c^r\rangle = 0 \qquad T > T_c \tag{2}$$

$$\langle c^r(\boldsymbol{R}) - c^r\rangle \neq 0 \qquad T \leqslant T_c.$$

We have $c^r = c^{r+3} = c = \frac{1}{3}$ for the concentration.

In second order in the displacements and the pseudo-spins the elastic energy of the system can be written as (Khatchaturian 1965)

$$E = \tfrac{1}{2}\sum_{\boldsymbol{R}\boldsymbol{R}'}\sum_{rs} J^{rs}(\boldsymbol{R}-\boldsymbol{R}')[c^r(\boldsymbol{R}) - c][c^s(\boldsymbol{R}') - c] + \tfrac{1}{2}\sum_{\boldsymbol{R}\boldsymbol{R}'} \boldsymbol{D}_{\mu\nu}(\boldsymbol{R}-\boldsymbol{R}')u^*_\nu(\boldsymbol{R})u_\mu(\boldsymbol{R}')$$

$$+ \sum_{\boldsymbol{R}\boldsymbol{R}'}\sum_r G^r(\boldsymbol{R}-\boldsymbol{R}')u(\boldsymbol{R})[c^r(\boldsymbol{R}) - c] \tag{3}$$

where $s,r = 1, \ldots, 6$. Here J^{rs} is a still unspecified direct interaction and $\mathbf{D}$ the tensor of the elastic moduli (double indices are summed over).

The linear coupling between the displacements and concentration fluctuations which contains the elastic dipoles will now be discussed more thoroughly.

It is well known (Khatchaturian 1966) that in the presence of an elastic dipole described by the tensor P in $\boldsymbol{R}_0$, the elastic energy density is given by

$$\varphi(\boldsymbol{R}) = P_{ij}\varepsilon_{ij}\theta(\boldsymbol{R}-\boldsymbol{R}_0) + \tfrac{1}{2}\lambda_{ijlm}\varepsilon_{ij}\varepsilon_{lm} \tag{4}$$

where the deformations ε_{ij} are defined as

$$\varepsilon_{ij} = \tfrac{1}{2}[\partial u_i(\boldsymbol{R})/\partial x_j + \partial u_j(\boldsymbol{R})/\partial x_i] \tag{5}$$

and $\theta(\boldsymbol{R}-\boldsymbol{R}_0)$ describes the range of the dipole (in a small volume V). Actually it is usual for Huang scattering to idealise:

$$\theta(\boldsymbol{R}-\boldsymbol{R}_0)/V \rightarrow \delta(\boldsymbol{R}-\boldsymbol{R}_0) \qquad \text{as } \boldsymbol{R}\rightarrow\boldsymbol{R}_0 \text{ and } V\rightarrow 0. \tag{6}$$

λ_{ijlm} are the elastic constants, which we will use in Voigt notation later on.

Comparing (3) and (4) one sees that together with (5)

$$G(\boldsymbol{R}-\boldsymbol{R}')\boldsymbol{u}(\boldsymbol{R}) = P_{ij}\left(\frac{\partial u_i}{\partial x_j}+\frac{\partial u_j}{\partial x_i}\right)\theta(\boldsymbol{R}-\boldsymbol{R}')/2. \tag{7}$$

Obviously it is convenient to transform (3) to $\boldsymbol{q}$-space, using (6) and expanding in (acoustic) normal modes

$$\boldsymbol{u}(\boldsymbol{R}) = (1/\sqrt{N})\sum_{\boldsymbol{q}}\sum_{j=1,2,3}[Q_j(\boldsymbol{q})\boldsymbol{e}_j(\boldsymbol{q})\mathrm{e}^{\mathrm{i}\boldsymbol{q}\cdot\boldsymbol{R}} + \mathrm{cc}] \tag{8}$$

($\boldsymbol{q}$ is in the first Brillouin zone, $\boldsymbol{e}_j(\boldsymbol{q})$ are the polarisation vectors) and using the eigenvalue equation for the lattice dynamical matrix:

$$\sum_{\boldsymbol{R}'} D_{\nu\mu}(\boldsymbol{R}-\boldsymbol{R}')e_j^{\mu}(\boldsymbol{q})\mathrm{e}^{\mathrm{i}\boldsymbol{q}\cdot\boldsymbol{R}'} = m\omega_j^2(\boldsymbol{q})e_j^{\nu}(\boldsymbol{q})\mathrm{e}^{\mathrm{i}\boldsymbol{q}\cdot\boldsymbol{R}} \tag{9}$$

(m is the mass of the mean lattice).

One further generalises to many dipoles, in $\boldsymbol{R}_n$, and the 2×3 types of distortive orientations, so that (3) becomes

$$E = \tfrac{1}{2}\sum_{\boldsymbol{q}}\sum_{r,s}J^{rs}(\boldsymbol{q})c^r(\boldsymbol{q})c^s(-\boldsymbol{q}) + \tfrac{1}{2}\sum_{\boldsymbol{q}}\sum_{j}m\omega_j^2(\boldsymbol{q})Q_j(\boldsymbol{q})Q_j(-\boldsymbol{q})$$
$$+\sum_{\boldsymbol{q}}\sum_{j}\sum_{r}i(P^r\boldsymbol{q}\cdot\boldsymbol{e}_j)Q_j(\boldsymbol{q})c^r(-\boldsymbol{q}). \tag{10}$$

The linear interaction which can now be thought of as a spin–phonon interaction has the form

$$h_j^r = i(P^r\boldsymbol{q}\cdot\boldsymbol{e}_j) \tag{11}$$

where—here we take over earlier results (Schotte 1987)—the P^r are given by

$$P^r = -v\left[c_{66}\begin{pmatrix}\hat{P}^r_{xx} & \hat{P}^r_{xy} & 0\\ \hat{P}^r_{yx} & \hat{P}^r_{yy} & 0\\ 0 & 0 & 0\end{pmatrix} + c_{44}\begin{pmatrix}0 & 0 & \hat{P}^r_{xz}\\ 0 & 0 & \hat{P}^r_{yz}\\ \hat{P}^r_{xz} & \hat{P}^r_{zy} & 0\end{pmatrix}\right] \tag{12}$$

and v is something like an effective dipole volume times the JT elongation of the octahedron axis (discussed again in § 5).

In the case of a Q_3 elongation of the Cu–Cl octahedron

$$\hat{P}^1 = \begin{pmatrix} 1 & 0 & \sqrt{2} \\ 0 & -1 & 0 \\ \sqrt{2} & 0 & 0 \end{pmatrix} \qquad \hat{P}^2 = \tfrac{1}{2}\begin{pmatrix} -1 & -\sqrt{3} & -\sqrt{2} \\ -\sqrt{3} & 1 & \sqrt{6} \\ -\sqrt{2} & \sqrt{6} & 0 \end{pmatrix}$$

$$\hat{P}^3 = \tfrac{1}{2}\begin{pmatrix} -1 & \sqrt{3} & -\sqrt{2} \\ \sqrt{3} & 1 & -\sqrt{6} \\ -\sqrt{2} & -\sqrt{6} & 0 \end{pmatrix} \qquad \hat{P}^4 = \begin{pmatrix} 1 & 0 & -\sqrt{2} \\ 0 & -1 & 0 \\ -\sqrt{2} & 0 & 0 \end{pmatrix} \tag{13}$$

$$\hat{P}^5 = \tfrac{1}{2}\begin{pmatrix} -1 & -\sqrt{3} & \sqrt{2} \\ -\sqrt{3} & 1 & -\sqrt{6} \\ \sqrt{2} & -\sqrt{6} & 0 \end{pmatrix} \qquad \hat{P}^6 = \tfrac{1}{2}\begin{pmatrix} -1 & \sqrt{3} & \sqrt{2} \\ \sqrt{3} & 1 & \sqrt{6} \\ \sqrt{2} & \sqrt{6} & 0 \end{pmatrix}.$$

These tensors were derived by rotating the Q_3-type tensors for tetragonal stretching:

$$\hat{P}_0^3 = \begin{pmatrix} -1 & 0 & 0 \\ 0 & -1 & 0 \\ 0 & 0 & 2 \end{pmatrix}$$

into the six equivalent positions in the hexagonal $ABCl_3$ crystal (figure 4).

We can restrict the treatment to Q_3-type octahedral stretching since the neutron scattering intensity always involves the P^r tensors in the combination

$$\sum_r P^r \otimes P^r \qquad \text{or} \qquad \sum_r P^r \otimes P^{r+3}$$

which is insensitive to using Q_2 or $\pm Q_3$ or combinations thereof. Note that

$$\sum_1^3 P^r = \sum_4^6 P^r = 0 \tag{14}$$

and for later use that for the averaged tensor products one has

$$\tfrac{1}{6}\sum_r^6 \hat{P}^r \otimes \hat{P}^r = A \otimes A + B \otimes B + C \otimes C + D \otimes D \tag{15}$$

and

$$\tfrac{1}{6}\sum_r^6 P^r \otimes P^r = v^2 c_{66}^2 (A \otimes A + B \otimes B) + v^2 c_{44}^2 (C \otimes C + D \otimes D) \tag{16}$$

where

$$A = \frac{1}{\sqrt{2}}\begin{pmatrix} 1 & 0 & 0 \\ 0 & -1 & 0 \\ 0 & 0 & 0 \end{pmatrix} \qquad B = \frac{1}{\sqrt{2}}\begin{pmatrix} 0 & 1 & 0 \\ 1 & 0 & 0 \\ 0 & 0 & 0 \end{pmatrix}$$

$$C = \begin{pmatrix} 0 & 0 & 1 \\ 0 & 0 & 0 \\ 1 & 0 & 0 \end{pmatrix} \qquad D = \begin{pmatrix} 0 & 0 & 0 \\ 0 & 0 & 1 \\ 0 & 1 & 0 \end{pmatrix}. \tag{17}$$

Equations (14) to (17) help when explicitly calculating $\Sigma_r|P^r\boldsymbol{q}\cdot\boldsymbol{e}_j|^2$ which will enter into the 'softened' frequency $\omega_{js}(\boldsymbol{q})$.

One can study the system from two sides: the pseudo-spins will be coupled via the strain field, and one can investigate the nature of these interactions and favourable low-T structures. The phonons will suffer damping and softening in the presence of the flipping spins, accessible experimentally to inelastic neutron scattering. The pseudo-spins are not directly 'visible' to the neutrons but from the inelastic scattering results a 'bare' and an 'effective' (in the elastic medium) flip rate will emerge; thus the neutron data from the high-T phase also yield information on the pseudo-spin interactions.

Through its T dependence the flip rate also contains information about the warping term of the Jahn–Teller cluster in the bulk system. In this respect the neutron investigations of the high-T (paradistortive) phase offer a unique possibility of approaching microscopic JT parameters in the bulk system, in contrast to the usually investigated non-JT systems with JT impurities (Reinen *et al* 1979).

In the next section the spin–spin interactions are discussed to get some ideas about possible ordered structures caused by phonon interactions alone; in § 4 the phonon correlation functions $\langle Q_iQ_j\rangle$, which enter into the neutron scattering cross sections, will be calculated.

3. Phonon-induced interaction between elastic dipoles

The effective pseudo-spin interaction is obtained by putting, in (10),

$$\partial E/\partial Q_j(-\boldsymbol{q}) = 0 \tag{18}$$

and solving for $Q_j(\boldsymbol{q})$:

$$Q_j(\boldsymbol{q}) = (1/m\omega_j^2)\sum_r i(P^r\boldsymbol{q}\cdot\boldsymbol{e}_j)c^r(\boldsymbol{q}) \tag{19}$$

and inserting in (10) to obtain an effective pseudo-spin energy

$$E_s^{\text{eff}} = \tfrac{1}{2}\sum_{\boldsymbol{q}}\sum_{rs}\left(J^{rs} - \sum_j \frac{(P^r\boldsymbol{q}\cdot\boldsymbol{e}_j)(P^s\boldsymbol{q}\cdot\boldsymbol{e}_j)}{m\omega_j^2}\right)c^r(\boldsymbol{q})c^s(-\boldsymbol{q}). \tag{20}$$

The phonon-mediated part of the effective interaction can be written as, with (9),

$$V^{rr'}(\boldsymbol{q}) = (P^r\boldsymbol{q}\cdot\mathbf{D}^{-1}(\boldsymbol{q})\cdot P^{r'}\boldsymbol{q}). \tag{21}$$

From (20), $V^{rr'}(\boldsymbol{R}) > 0$ means ferrodistortive and $V^{rr'}(\boldsymbol{R}) < 0$ antiferrodistortive interactions.

Fourier-transforming back to real space one has

$$\begin{aligned} V^{rr'}(\boldsymbol{R}-\boldsymbol{R}') &= [P^r\nabla_{\boldsymbol{R}}\cdot\nabla_{\boldsymbol{R}'}P^{r'}\mathbf{D}^{-1}(\boldsymbol{R}-\boldsymbol{R}')] \\ &= P^r_{mk}P^{r'}_{nl}\frac{\partial^2}{\partial R_m\,\partial R'_n}\boldsymbol{D}^{-1}_{kl}(\boldsymbol{R}-\boldsymbol{R}') \end{aligned} \tag{22}$$

with

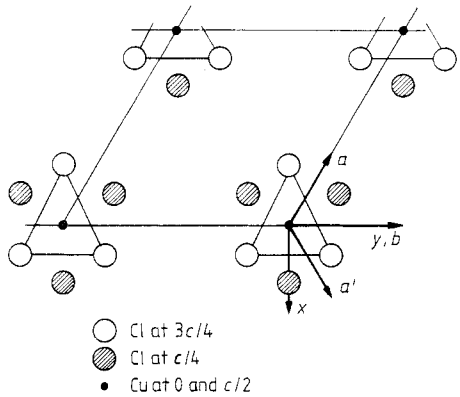

Figure 5. Hexagonal plane with Cu and Cl positions indicated. To fit the model of figure 4(*a*) into the real lattice, the double octahedron is shifted by $c/4$ upwards along z.

$$\mathbf{D}^{-1}(\boldsymbol{R}-\boldsymbol{R}') = N^{-1/2}\sum_{q}\exp[-i\boldsymbol{q}\cdot(\boldsymbol{R}-\boldsymbol{R}')]D_{kl}^{-1}(\boldsymbol{q}). \tag{23}$$

Since $\mathbf{D}^{-1} \sim q^{-2}$ the modulus of $\boldsymbol{q}$ drops out of (21), which means that in $\boldsymbol{R}$-space

$$V^{rr'}(\boldsymbol{R}-\boldsymbol{R}') \sim |\boldsymbol{R}-\boldsymbol{R}'|^{-3}. \tag{24}$$

Obviously there is a strong angular or directional dependence in $\boldsymbol{q}$- as well as in $\boldsymbol{R}$-space.

These well-known features of dipole systems lead, for example, to the lattice sum

$$V^{rr'}(0) = \sum_{\boldsymbol{R}\neq\boldsymbol{R}'} V^{rr'}(\boldsymbol{R}-\boldsymbol{R}') \tag{25}$$

being badly convergent or rather depending on the sample shape. This has interesting consequences, especially for predominantly ferrotype interactions: the energy is lowered by domain formation with optimal shapes depending on crystal symmetry. For solid solutions this is extensively discussed by de Fontaine (1979) and (in a spirit more related to ours) for compounds—the alkali cyanides—by de Raedt *et al* (1981). For our purpose we note that the dipolar forces have two outstanding properties, their long range and their directional dependence. While the former seems favourable for molecular-field theory to work, the latter makes the force effectively short-range, *grosso modo* because cancellations occur as in (25). This can be expressed by an effective number of nearest neighbours which can be surprisingly small (Friedman and Felsteiner 1974). Therefore speculations about low-T structures from cluster energies are allowed but molecular-field results will be less reliable.

The main obstacle for the discussion of $V^{rr'}(\boldsymbol{R}-\boldsymbol{R}')$ is $\mathbf{D}^{-1}(\boldsymbol{R}-\boldsymbol{R}')$; although in principle known for hexagonal systems, it is very tedious to work with. Also we would need the elastic constants at high temperatures $T \gg T_c$. Important information, especially about the sign of the interactions in high-symmetry directions, can also be won by treating the system as isotropic. Then, with one dipole in $\boldsymbol{R}' = 0$, the other at distance r in $\boldsymbol{R}$, one uses (Landau and Lifshitz 1965 vol VII)

$$D_{kl}^{-1}(\boldsymbol{R}, 0) = [1/16\pi\mu(1-\sigma)][4(1-\sigma)\delta_{kl}/r + R_kR_l/r^3] \tag{26}$$

with $\mu = (c_{11}-c_{12})/2$ the shear modulus and $\sigma = c_{12}/(c_{11}+c_{12})$ the Poisson number with $0 < \sigma < 0.5$ (for our systems σ is close to 0.3).

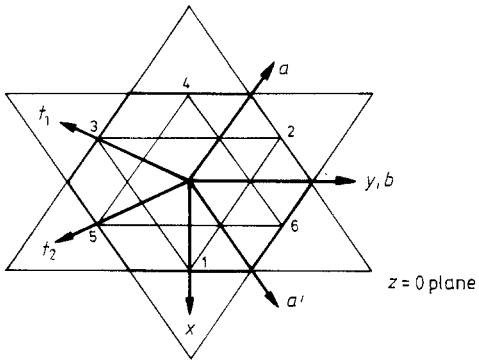

Figure 6. Taking the right lower corner of figure 5 as centre, the directions towards nearest (a, b, a') and next-nearest (t_1, t_2 and x) neighbours are shown. Also the relative orientation of the basic triangles of distorted octahedra can be deduced.

We use for short

$$\boldsymbol{D}_{kl}^{-1}(\boldsymbol{R}) = a\,\delta_{kl}/r + b\,R_k R_l/r^3 \qquad \text{with } 2 < a/b < 4. \tag{27}$$

Note that

$$\frac{\partial}{\partial R'_m}\mathbf{D}^{-1}(\boldsymbol{R}-\boldsymbol{R}') = -\frac{\partial}{\partial R_m}\mathbf{D}^{-1}(\boldsymbol{R}-\boldsymbol{R}'). \tag{28}$$

For the dipole tensors the forms $\hat{P}^r$, equations (13), can be used since in an isotropic medium $\mu = c_{66} = c_{44}$, so that instead of (12)

$$P^r = v\mu\hat{P}^r. \tag{29}$$

The interactions

$$\begin{aligned} V^{rr'}(R) &= -P^r_{mk}P^{r'}_{nl}\,\partial^2\boldsymbol{D}^{-1}_{kl}(\boldsymbol{R})/\partial R_n\,\partial R_m \\ &\equiv -P^r_{mk}P^{r'}_{nl}\boldsymbol{D}^{kl}_{nm} \end{aligned} \tag{30}$$

have now to be calculated for directions from the coordinate origin (where octahedron type r resides) along which one finds nearest and next nearest neighbours, the latter because, for three-state pseudo-spins with antiferro coupling, one has two options for the type of nearest neighbour and the next nearest may enable a decision between them.

The interactions (30) contain various information: about the symmetry, about the elastic medium influence and of course about the sign. Before going into these let us again make the nomenclature clear. In figure 4 the coordinate system used for the two basic octahedra is shown; the explicit form of the P^r depends on it. In figure 5 it is shown how the objects of figure 4 are situated in the hexagonal plane of the lattice. When we investigate interactions along c, figure 2 can be consulted. Distortions 1, 2, 3 refer to the lower octahedron; if from point 1 the axis upwards is stretched, the elastic dipole is described by P^1; if from point 4 in the upper octahedron the upgoing axis is stretched, we deal with P^4.

We proceed to calculate nearest- and next-nearest-neighbour interactions in a basic hexagon. Six $\boldsymbol{R}$ directions have to be considered, which are however not independent of each other (see figure 6).

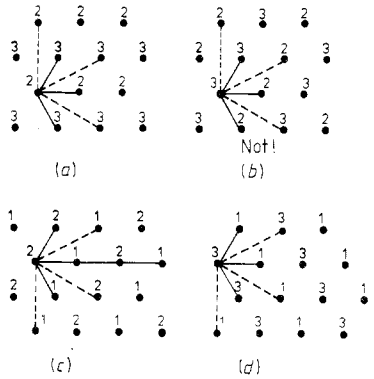

Figure 7. Energetically favourable (*a*), (*c*), (*d*) and unfavourable (*b*) neighbourhoods resulting from direction-dependent dipole–dipole interactions in the hexagonal plane (broken lines to next-nearest neighbours).

From $V_b^{rr'}$ for $\boldsymbol{R} = (0, y, 0) \| b$ one can deduce the interaction matrix for $\boldsymbol{R} = (\sqrt{3}x, \pm x, 0)$ along a and a' by renumbering the distortions in figure 4(*b*). Also $V^{rr'}(x, 0, 0)$ has to be calculated, then the values for $\boldsymbol{R}$ along t_1 and t_2, parallel to the two other next-nearest directions, can be deduced.

Along x and y the few derivatives $\boldsymbol{D}_{nm}^{kl}$ that occur are rather trivial to calculate. Here is the result for $V_b^{rr'} \equiv V^{rr'}(0, y, 0)$:

$$V_b^{11} \equiv V^{11} = (v\mu)^2 (3a - 12b)/y^3 < 0 \tag{31}$$

$$V_b^{22} = V_b^{33} \equiv V^{22} = (v\mu)^2 (51b/4 - 3a/2)/y^3 > 0 \tag{32}$$

$$V_b^{12} \equiv V_b^{13} = -V^{11}/2 = (v\mu)^2 (6b - 3a/2)/y^3 > 0. \tag{33}$$

From this and symmetry considerations for $V_a^{rr'}$ and $V_{a'}^{rr'}$, the following interaction matrices result (rows are labelled $r = 1, 2, 3$ and columns $r' = 1, 2, 3$):

$$V_b^{rr'} = \begin{pmatrix} V^{11} & -V^{11}/2 & -V^{11}/2 \\ -V^{11}/2 & V^{22} & V^{11}/2 - V^{22} \\ -V^{11}/2 & V^{11}/2 - V^{22} & V^{22} \end{pmatrix}$$

$$V_a^{rr'} = \begin{pmatrix} V^{22} & V^{11}/2 - V^{22} & -V^{11}/2 \\ V^{11}/2 - V^{22} & V^{22} & -V^{11}/2 \\ -V^{11}/2 & -V^{11}/2 & V^{11} \end{pmatrix} \tag{34}$$

$$V_{a'}^{rr'} = \begin{pmatrix} V^{22} & -V^{11}/2 & V^{11}/2 - V^{22} \\ -V^{11}/2 & V^{11} & -V^{11}/2 \\ V^{11}/2 - V^{22} & -V^{11}/2 & V^{22} \end{pmatrix}.$$

One sees that in the hexagonal plane it happens that the sign of the interaction depends on the direction of the vector joining the two elastic dipoles. Therefore antiferrodistortively ordered rows of in themselves ferro-ordered distortions can occur with anisotropy in the plane, as shown in examples in figure 7.

A closer look at the size of the interaction involved shows that pure ferrodistortive order can be preferred, depending on the elastic constants. The energies of the triangles (figures 8(*a*) and(*b*)) are, respectively,

$$V_b^{22} + V_a^{23} + V_{a'}^{23} = V^{22} - V^{11} = w(24.25b - 4.5a) \tag{35a}$$

$$V_b^{11} + V_a^{11} + V_{a'}^{11} = 2V^{22} + V^{11} = 13bw \tag{35b}$$

with $w = (\mu v)^2/y^3$. Considering $2 < a/b < 4$, one sees that both arrangements are possible and at $a/b = 2.5$ the energies are equal.

For next-nearest neighbours in the hexagonal plane one finds comparable circumstances: along $R_x = (x, 0, 0)$ with $x = \sqrt{3}a$

$$V_x^{11} = [(v\mu)^2/|x|^3](6b - 5a) < 0 \tag{36}$$

which means antiferrodistortive, but

$$V_x^{22} = V_x^{33} = [(v\mu)^2/|x|^3](\tfrac{15}{4}\, b + a) \tag{37}$$

is always positive.

Interaction matrices similar to (34) can now be constructed with

$$\begin{aligned} V_{t_1}^{33} &= V_{t_2}^{22} = V_x^{11} < 0 \\ V_{t_1}^{11} &= V_{t_1}^{22} = V_x^{22} > 0 \\ V_{t_2}^{11} &= V_{t_2}^{33} = V_x^{22} \end{aligned} \tag{38}$$

and the mixed elements $V_t^{rr'}$ according to (34). It is not surprising that from next-nearest interactions the configurations (*a*), (*c*), (*d*) of figure 7 are equivalent, $\Sigma V_i = 2(V_x^{22} - V_x^{11}) > 0$, while for (*b*) $\Sigma V_i = 0$, which is less favourable.

All that has been said for $V^{rr'}$, $r, r' = 1, 2, 3$ holds for $V^{rr'}$, $r, r' = 4, 5, 6$; one just puts $r \rightarrow r + 3$.

Along the *c* direction, $\boldsymbol{R} = (0, 0, z)$, the most important one is the nearest-neighbour inter-lattice interaction, because the distance is only $c/2$ while the other factors are of comparable magnitude.

Along *c* one has a simple three-states Potts model because the interaction matrices, also for the next-nearest neighbours, have the form

$$V_c^{rr'}(V_c^{rr'+3}) = \begin{pmatrix} V & -V/2 & -V/2 \\ -V/2 & V & -V/2 \\ -V/2 & -V/2 & V \end{pmatrix} \tag{39}$$

(where as before rows are labelled $r = 1, 2, 3$ for $V_c^{rr'}$ and 4, 5, 6 for $V_c^{rr'+3}$ and columns are labelled $r' = 1, 2, 3$). The result for 'joining stretched axes' is

$$V_c^{14} = V_c^{25} = V_c^{36} = [(\mu v)^2/|z|^3](4a - 16b) < 0 \tag{40}$$

which corresponds to the 'axis avoiding correlation' and to the observation that stretched axes never meet at the same anion in the low-T structures.

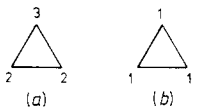

Figure 8. Smallest cluster for ferrodistortive row-wise ordering like in figure 7 and for purely ferrodistortive ordering.

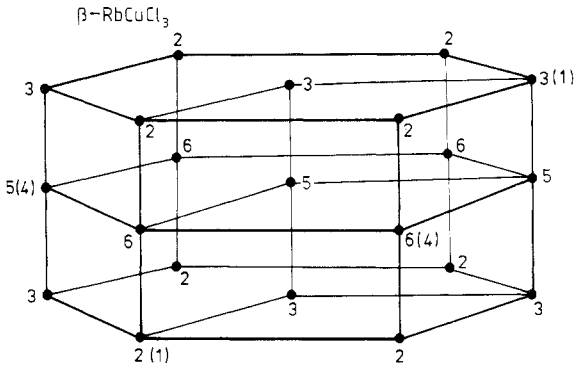

Figure 9. Intermediate phase of $RbCuCl_3$ (with 'impurities') as proposed by Tanaka *et al* (1986a), consistent with the deduced dipolar interactions.

For the next-nearest neighbours along c one has (at $z = c$)

$$V_c^{11} = V_c^{22} = V_c^{33} = [(v\mu)^2/|z|^3]\,12b > 0. \tag{41}$$

This means we have a three-states Potts model with antiparallel coupling between nearest neighbours and parallel ordering tendencies for distortions of the same type at next-nearest-neighbour sites.

This makes plausible a structure which has been suggested for β-$RbCuCl_3$ consisting of 3535... and 2626... chains arranged in agreement with figure 7, shown in figure 9. According to the somewhat ambiguous structural information, Tanaka *et al* suggest additional disorder (indicated in figure 9 by numbers in parentheses) such that a few distortions 1 or 4 occur randomly, averaging to an overall Q_2 instead of Q_3 ordering in the planes (for details see Tanaka *et al* 1986a).

For β-$RbCrCl_3$ a structure with partly ordered c-chains is suggested, for example $4(\frac{2}{3})4(\frac{2}{3})$ such that ordered planes alternate with Ising-type disordered planes. It has been shown (Samukhin 1982) that in a cubic system a three-state Potts model with antiferro-type interactions along c and a ferro-type interaction in the basal plane (just one!) has such a structure as a possible ground state. A parallel can be drawn if one has isotropic tendencies (figure 8(b)) in the plane.

It could be that $V_c^{rr'}$ is of comparable size for the third-neighbour interactions $V_d^{rr'}$ with (one of them) $R = (0, y, cy/2a)$ at distance $r = \sqrt{(a^2 + c^2/4)} \simeq 7.8$ Å ($a = 7.2$ Å; $c = 6.1$ Å). By studying the non-zero 'odd' derivatives, like $\boldsymbol{D}_{xz}^{xy}$ and the explicit shapes of $P^r \otimes P^{r'+3}$ one can easily find the general form for V_d^{rs} ($r = 1, 2, 3$; $s = 4, 5, 6$):

$$V_d^{rs} = \begin{pmatrix} V^{14} & -V^{14}/2 - \alpha & -V^{14}/2 + \alpha \\ -V^{14}/2 + \alpha & V^{14}/4 + \beta & V^{14}/4 - \beta - \alpha \\ -V^{14}/4 - \alpha & V^{14}/2 - \beta + \alpha & V^{14}/4 + \beta \end{pmatrix}. \tag{42}$$

Note that $V_d^{15} \neq V_d^{16}$ so that the symmetry of V_c^{rs}, equation (39), gets lowered.

Since there are 12 third-nearest neighbours or six different directions to be considered, the situation becomes quite involved. The isotropic model no longer seems good enough if several options arise depending on the size of the elastic constants.

In conclusion these simple calculations show that the pseudo-spin interactions oscillate in sign and decay with distance similar to Rudermann–Kittel interactions, along c,

while in the hexagonal plane they oscillate or just decay. From this it is easy to anticipate as favourable low-T structures those of the β-phase of the Rb compounds where doubling or tripling of the lattice cell along c is not yet involved. The latter implies balancing the tendency of next-nearest neighbours to order ferrodistortively against that to undergo bulk distortions (monoclinic angle); obviously the ferrotype interaction works against an even distribution of the six orientations of the basic elastic dipole. $CsCuCl_3$ in its low-T phase shows the only possible realisation of the 'axis avoiding correlation' and zero monoclinic angle because each elastic dipole appears just once in the unit cell, in the c-chains 16243516... or 34261534....

4. The phonon correlation function and inelastic neutron scattering cross section

Since we aim at a quantitative description of the neutron results, it will be helpful to list the essentials about acoustic phonons in the hexagonal system which enter into the discussion of the softening of certain elastic constants. One can always choose the coordinate system such that $\boldsymbol{q}$ is in the x^*z^*-plane and q_z is along $z^* \| c^*$. For the sound velocities and polarisation vectors, one has to find the eigenvalues and eigenvectors of

$$\boldsymbol{D} = \begin{pmatrix} \boldsymbol{D}_{xx} & 0 & \boldsymbol{D}_{zx} \\ 0 & \boldsymbol{D}_{yy} & 0 \\ \boldsymbol{D}_{zx} & 0 & \boldsymbol{D}_{zz} \end{pmatrix} \tag{43}$$

with

$$\begin{aligned} \boldsymbol{D}_{xx} &= c_{11}q_x^2 + c_{44}q_z^2 \qquad & \boldsymbol{D}_{yy} &= c_{66}q_x^2 + c_{44}q_z^2 \\ \boldsymbol{D}_{zz} &= c_{33}q_z^2 + c_{44}q_x^2 \qquad & \boldsymbol{D}_{zx} &= (c_{13} + c_{44})q_xq_z. \end{aligned} \tag{44}$$

The eigenvalue equation

$$\det(\mathbf{D} - \rho\omega^2) = 0 \tag{45}$$

has the solution

$$\rho\omega_{1/3}^2 = (\boldsymbol{D}_{xx} + \boldsymbol{D}_{zz})/2 \mp [(\boldsymbol{D}_{xx} - \boldsymbol{D}_{zz})^2 + 4\boldsymbol{D}_{xz}^2]^{1/2}/2 \tag{46}$$

$$\rho\omega_2^2 = \boldsymbol{D}_{yy} \tag{47}$$

and the eigenvectors in

$$\mathbf{D}\boldsymbol{e}_j = \rho\omega_j^2\boldsymbol{e}_j \tag{48}$$

have the shape

$$\begin{aligned} \boldsymbol{e}_1 &= (-b(\boldsymbol{q}), 0, a(\boldsymbol{q})) \\ \boldsymbol{e}_2 &= (0, 1, 0) \\ \boldsymbol{e}_3 &= (a(\boldsymbol{q}), 0, b(\boldsymbol{q})) \end{aligned} \tag{49}$$

with $a^2(\boldsymbol{q}) + b^2(\boldsymbol{q}) = 1$ so that they are orthonormalised. One can choose

$$\begin{aligned} a(\boldsymbol{q}) &= (\boldsymbol{D}_{zz} - \rho\omega_3^2)/[\boldsymbol{D}_{xz}^2 + (\boldsymbol{D}_{zz} - \rho\omega_3^2)^2]^{1/2} \\ b(\boldsymbol{q}) &= -\boldsymbol{D}_{xz}/[\boldsymbol{D}_{xz}^2 + (\boldsymbol{D}_{zz} - \rho\omega_3^2)]^{1/2}. \end{aligned} \tag{50}$$

We list the interesting limits $\boldsymbol{q} = (q_x, 0, 0)$:

$$\begin{aligned} \rho\omega_1^2 &= c_{44}q_x^2 \qquad & \boldsymbol{e}_1 &= (0, 0, 1) \qquad & \text{TA} \\ \rho\omega_2^2 &= c_{66}q_x^2 \qquad & \boldsymbol{e}_2 &= (0, 1, 0) \qquad & \text{TA} \\ \rho\omega_3^2 &= c_{11}q_x^2 \qquad & \boldsymbol{e}_3 &= (1, 0, 0) \qquad & \text{LA} \end{aligned} \tag{51}$$

and $\boldsymbol{q} = (0, 0, q_z)$:

$$\begin{aligned} &\rho\omega_{2/3}^2 = c_{44}q_z^2 && \boldsymbol{e}_2 = (0,1,0) && \text{two degenerate TA} \\ &&& \boldsymbol{e}_3 = (1,0,0) && \\ &\rho\omega_1^2 = c_{33}q_z^2 && \boldsymbol{e}_1 = (0,0,1) && \text{LA.} \end{aligned} \tag{52}$$

When we use the elastic matrix as above a factor ρ/m will appear in

$$\sum_i \frac{(\boldsymbol{a}\cdot\boldsymbol{e}_i)(\boldsymbol{e}_i\cdot\boldsymbol{b})}{m\omega_i^2} = \frac{\rho}{m}(\boldsymbol{a}\cdot\mathbf{D}^{-1}\boldsymbol{b}) \tag{53}$$

where $m^{-1} = 0.2m_{\mathrm{Cs}}^{-1} + 0.2m_{\mathrm{Cu}}^{-1} + 0.6m_{\mathrm{Cl}}^{-1}$. We use $\rho/m = 3.62/(77.4 \times 10^{-24})\ \mathrm{cm}^{-3}$.

We apply and extend the method of Yamada *et al* (1974) who calculate the correlation function as the time-correlated thermodynamic fluctuation of the elastic deformations (the latter expressed by phonon amplitudes), the Fourier transform of which enters in the inelastic neutron scattering cross section. This is a classical method valid for high temperatures, and the ingredients of it are also found in Landau and Lifshitz (1965, vol V). We therefore only sketch the method. Consider the state vector

$$\boldsymbol{X} = (p_1, p_2, p_3, Q_1, Q_2, Q_3, c^1(\boldsymbol{q}), c^2(\boldsymbol{q}), \ldots, c^6(\boldsymbol{q})) \tag{54}$$

made up of the variables of the energy (10) and the conjugate momenta p_j. What we need is

$$\varphi_{ij}(\tau) = \langle x_i(t+\tau)x_j(\tau)\rangle \tag{55}$$

where x_j, x_i are components of $\boldsymbol{X}$. The thermodynamic fluctuation $\varphi_{ij}(0) \equiv \langle x_i x_j\rangle$ is given by a Gaussian average

$$\varphi_{ij}(0) = [\beta^{1/2}/(2\pi)^{2/3}] \int \ldots \int x_i x_j \exp(-\beta_{lm}x_l x_m)\,\mathrm{d}x_1 \ldots \mathrm{d}x_n \tag{56}$$

with $\beta = \det(\beta_{ij})$ and with the free energy $(E - TS)$ in the exponent. It can be proved that

$$\langle x_i x_j\rangle = \beta_{ij}^{-1}. \tag{57}$$

The rank of the matrix β_{ij} to be inverted is the number of components of $\boldsymbol{X}$.

In order to obtain the coefficients β_{lm} in the exponent of (56), we extend the expression for the energy (7) by the kinetic energy and the entropy. In order to determine the entropy to second order in $c^r(\boldsymbol{q})$, we remember that $c^r(\boldsymbol{q})$ is the Fourier transform of the order parameter $c^r(\boldsymbol{R}) - c^r \equiv \Delta c^r(\boldsymbol{R})$; see (1) and (2).

Expanding, we obtain

$$-TS = kT\sum_{r,\boldsymbol{R}} c^r(\boldsymbol{R}) \ln c^r(\boldsymbol{R}) = kT\sum_{r,\boldsymbol{R}} 3[\Delta c^r(\boldsymbol{R})]^2 + \text{const} + \ldots \tag{58}$$

and neglecting the third-order term which has to appear for a three-state spin and is usually responsible for the first-order transition, one obtains

$$F = E - TS \equiv kT\beta_{lm}x_l x_m = \tfrac{1}{2}\sum_{\boldsymbol{q},j} p_j(\boldsymbol{q})p_j(-\boldsymbol{q}) + \tfrac{1}{2}\sum_{\boldsymbol{q},j}\omega_j^2 Q_j(\boldsymbol{q})Q_j(-\boldsymbol{q})$$

$$+ \sum_{\boldsymbol{q}jr} h_j^r(\boldsymbol{q})Q_j(\boldsymbol{q})c^r(-\boldsymbol{q}) + \tfrac{1}{2}\sum_{\boldsymbol{q}r}(J^{rr} + 6kT)c^r(\boldsymbol{q})c^r(-\boldsymbol{q})$$

$$+ \tfrac{1}{2} \sum_{qr} J^{rr+3} c^r(\boldsymbol{q}) c^{r+3}(-\boldsymbol{q}) \tag{59}$$

with $h_j^r = i(P^r \boldsymbol{q} \cdot \boldsymbol{e}_j)/m^{1/2}$, from which one can read off the elements β_{ij} of the matrix β.

In order to calculate (55) one needs the time dependence of $x_j(\tau)$; one assumes

$$\dot{x}_j(\tau) = -\sum_k \lambda_{ik} x_k(\tau). \tag{60}$$

For the p_j and Q_j canonical equations of motions hold (therefore we have replaced $\sqrt{m}\,Q$ by Q when going from (10) to (59)), while

$$\dot{c}^r(q) = -\gamma[\Sigma h_j^r(-q) Q_j(-q) + (6kT + J^{rr}) c^r(-q) + J^{rr+3} c^{r+3}(-q)] \tag{61}$$

is taken with a constant relaxation rate γ. We will come back to the meaning of γ.

Then one can calculate (see Landau and Lifshitz 1965, vol V)

$$\langle x_i x_j \rangle_\omega = (1/2\pi) \int_{-\infty}^{\infty} \varphi_{ij}(\tau)\, \mathrm{e}^{\mathrm{i}\omega\tau}\, \mathrm{d}\omega$$

$$= (1/\pi)\, \mathrm{Re}(\beta\lambda - \mathrm{i}\omega\beta)^{-1}_{ij}. \tag{62}$$

Although the matrices β, λ and $\beta\lambda$ are easy to write down, from (59), (60) and (61) it is quite tedious to calculate $\langle Q_i Q_j \rangle_\omega$ since for the full problem one has to invert a 12×12 matrix.

The problem is solved in steps. For one phonon mode ω_0 coupled to one sublattice of pseudo-spins one easily extends the results of Yamada *et al* (1974):

$$\langle QQ \rangle_\omega = \gamma(kT/\pi)\, (h/\gamma\tilde{J})^2 / [(\omega^2 - \omega_0^2 + h^2/\tilde{J})^2 + \omega^2(\omega^2 - \omega_0^2)^2/(\gamma\tilde{J})^2] \tag{63}$$

where

$$\tilde{J} = 6kT + J \qquad h^2 = \sum_r |P^r \boldsymbol{q} \cdot \boldsymbol{e}_0|^2/m.$$

Equation (63) has the popular 'three-pole' structure, that is, as a function of ω it shows humps at $\omega^2 = \omega_s^2 = \omega_0^2(1 - h^2/\tilde{J}\omega_0^2)$ or $\omega^2 \simeq \omega_0^2$ and $\omega = 0$; which ones are most pronounced depends also on $\boldsymbol{q}$ in $\rho\omega_0^2 = cq^2$, or more precisely on the ratio $\omega_0^2/(\gamma\tilde{J})^2$ (c is the relevant elastic modulus).

For the two-sublattices problem, which comes in through the last term in (59), we assume a simple three-state Potts model, i.e. one without the directional dependences of $V^{rr'}$ discussed in the last section but one with interactions like in (39), which should be acceptable for the nearest-neighbour inter-lattice interaction J^{rr+3}. Then the elastic limit of the phonon correlation function is easy to find:

$$\langle QQ \rangle_{\omega=0} = \frac{kT}{\gamma\pi} \frac{(\bar{J}^2 + V^2) \sum |h^r|^2 - 2\bar{J}V \sum h^r(\boldsymbol{q}) h^{r+3}(-\boldsymbol{q})}{(\bar{J}^2 - V^2)^2 \left[\omega_0^2 - \left(\bar{J} \sum |h^r|^2 - V \sum h^r h^{r+3} \right) \Big/ (\bar{J}^2 - V^2) \right]^2} \tag{64}$$

where $\bar{J} = J^{rr} + 6kT$ and $V = J^{rr+3}$ (independent of r).

Obviously, the 'axes avoiding correlation' contained in $h^r h^{r+3}$ occurs only when J^{rr+3} is 'switched on'. We will show below that $\langle QQ \rangle_{\omega=0}$ is closely related to quasi-elastic

'dense Huang scattering' where a contribution proportional to $\Sigma P^r \otimes P^{r+3}$ appeared when short-range correlations along c were explicitly inserted (Schotte 1987). In the spirit of the last section, V should be more important than J^{rr} since nearest neighbours for the inter-lattice interaction are at distance $c/2$ compared to a or c for J^{rr}. Owing to the symmetry of $\Sigma P^r \otimes P^{r+3}$ different from $\Sigma P^r \otimes P^r$, there should be an observable influence on the shape of Huang iso-intensity contours. (No superstructure precursor diffuse peaks are expected from nearest-neighbour interactions alone.) Since no such influence could be observed, it is reasonable to ignore V and especially J^{rr}, as not relevant for the present situation immediately above T_c of $CsCuCl_3$, and to believe that the indirect elastic dipole interactions via the strain field dominate. Terauchi *et al* (1972) come to similar conclusions when discussing diffuse scattering in the high-temperature phase of $NiCr_2O_4$.

Consequently, in the high-T phase the neutrons cannot distinguish between a one-site-per-cell model with a six-component spin and a two-site-per-cell model with a three-component spin on each site. (In Schotte (1987) there is an error in equation (18): $\delta_{sr}c(1-c)$ has to be replaced by $c(\delta_{sr}-c)$. The consequence is a factor $\frac{1}{6}$ in front of the Huang scattering expression for both models.)

The calculation of $\langle Q_i Q_j \rangle_\omega$ for three acoustic phonons ω_1^2, ω_2^2, ω_3^2, which in the main symmetry directions are proportional to c_{44}, c_{66}, c_{33} and c_{11} (see equations (51) and (52)), starts from

$$E - TS = \tfrac{1}{2}(\omega_1^2 Q_1^2 + \omega_2^2 Q_2^2 + p_1^2 + p_2^2) + h_1 Q_1 S + h_2 Q_2 S + \tfrac{1}{2}kTS^2 \tag{65}$$

that is two phonons and one spin.

The result already extended to three phonons and six spin components is, for example for Q_1:

$$\langle Q_1 Q_1 \rangle_\omega = \frac{kT}{\pi} \frac{h_1^2/\gamma\bar{T}^2}{[\omega^2 - \omega_1^2 + \Sigma(\omega)]^2 + \omega^2(\omega^2 - \omega_1^2)^2/(\gamma\bar{T})^2} \tag{66}$$

with

$$\Sigma(\omega) = \frac{h_1^2}{\bar{T}} + \frac{h_2^2}{\bar{T}} \frac{\omega^2 - \omega_1^2}{\omega^2 - \omega_2^2} + \frac{h_3^2}{\bar{T}} \frac{\omega^2 - \omega_1^2}{\omega^2 - \omega_3^2}$$

with

$$\bar{T} = 6kT \qquad h_i^2 = \sum_r |P^r \boldsymbol{q} \cdot \boldsymbol{e}_i|^2/m. \tag{67}$$

Note that one has still mainly a 'three-pole structure', i.e. maxima of $\langle Q_1 Q_1 \rangle_\omega$ at $\omega \simeq \omega_1$, $\omega = \omega_{s1}$ and $\omega = 0$, but also zeros at $\omega = \omega_2$ and $\omega = \omega_3$, which leads to non-Lorentzian shapes when say ω_2 is close to ω_1 (or $\sqrt{c_{44}} \simeq \sqrt{c_{66}}$) for $\boldsymbol{q} = (q_x, 0, 0)$, and in addition there are further peaks discussed below and in figures 10 and 11.

Including the mixed correlations, the general result can be expressed as

$$\langle Q_i Q_j \rangle_\omega = \frac{kT}{\pi} \times \frac{h_i(\boldsymbol{q}) h_j(-\boldsymbol{q})/\gamma\bar{T}^2}{(\omega^2 - \omega_i^2)(\omega^2 - \omega_j^2)\{[1 + \Sigma_l |h_l(\boldsymbol{q})|^2/\bar{T}(\omega^2 - \omega_l^2)]^2 + \omega^2/(\gamma\bar{T})^2\}}. \tag{68}$$

This goes into the neutron scattering cross section

$$\mathrm{d}^2\sigma/\mathrm{d}\omega\mathrm{d}q = |\bar{b}|^2 \sum_{ij} (1/m)(\boldsymbol{K} \cdot \boldsymbol{e}_i)(\boldsymbol{K} \cdot \boldsymbol{e}_j)\langle Q_i Q_j \rangle_\omega \tag{69}$$

where the greater part of the dynamical structure factor including the Debye–Waller

factor, scattering power and cell contents is lumped into $\bar{b}$. For $\boldsymbol{K}$, one takes as a good approximation the Bragg indices; actually the scattering vector $\boldsymbol{Q} = \boldsymbol{K} + \boldsymbol{q}$ is meant. The final result for the neutron experiment is

$$\frac{\mathrm{d}^2\sigma}{\mathrm{d}q\mathrm{d}\omega} = |\bar{b}|^2 \frac{1}{\pi\gamma\bar{T}} \frac{1}{6} \sum_r \left| \sum_i \frac{(\boldsymbol{K}\cdot\boldsymbol{e}_i)(P^r\boldsymbol{q}\cdot\boldsymbol{e}_i)}{m(\omega^2-\omega_i^2)} \right|^2 \Xi(q,\omega,T) \tag{70}$$

with

$$\Xi^{-1}(q,\omega,T) = \left[1 + \sum_r \sum_j |P^r\,\boldsymbol{q}\,.\,\boldsymbol{e}_j|^2/m\bar{T}(\omega^2-\omega_j^2)\right]^2 + \omega^2/(\gamma\bar{T})^2.$$

For $\omega = 0$

$$\left(\frac{\mathrm{d}^2\sigma}{\mathrm{d}q\,\mathrm{d}\omega}\right)_{\omega=0} = |\bar{b}|^2 \frac{1}{6\pi\gamma\bar{T}} \frac{\rho}{m} \sum_r |\boldsymbol{K}\cdot\mathbf{D}^{-1}P^r\boldsymbol{q}|^2 \frac{1}{[1-\rho\Sigma_r(P^r\boldsymbol{q}\cdot\mathbf{D}^{-1}P^r\boldsymbol{q})/m\bar{T}]^2}. \tag{71}$$

If quasi-elastic scattering is interpreted as integrating over a well developed narrow Lorentzian peak near $\omega = 0$ (in (70) put all $\omega = 0$ except that in $\omega^2/(\gamma\bar{T})^2$):

$$\int \frac{\mathrm{d}^2\sigma}{\mathrm{d}q\,\mathrm{d}\omega}\mathrm{d}\omega \sim \tfrac{1}{6}\sum_r |\boldsymbol{K}\cdot\mathbf{D}^{-1}P^r\boldsymbol{q}|^2 \int \frac{6\gamma kT\,\mathrm{d}\omega/\pi}{[6\gamma kT(1-T_0/T)]^2+\omega^2}$$

$$= \tfrac{1}{6}\sum_r |\boldsymbol{K}\cdot\mathbf{D}^{-1}P^r\boldsymbol{q}|^2 \frac{1}{1-T_0(\boldsymbol{q})/T} \tag{72}$$

with

$$\frac{T_0}{T} = \frac{\rho}{6m}\sum_r \frac{(P^r\boldsymbol{q}\,.\,\mathbf{D}^{-1}P^r\boldsymbol{q})}{kT} \tag{73}$$

which is—apart from the temperature dependence—the expected Huang result. Actually, depending on the width of the central component compared to the experimental resolution, (71) as well as (72) might have been seen.

From (72) the width of the central line goes to zero as $T \to T_0$, i.e.

$$\Gamma_{\text{centre}} = 6\gamma k(T - T_0) \tag{74}$$

and the maximum intensity at $\omega = 0$, from (71), behaves as $T/(T-T_0)^2$, while the integrated quasi-elastic intensity from (72) is proportional to $T/(T-T_0)$.

Note that T_0 refers to a second-order displacive phase transition at a temperature (as we will find below, about 40 K) lower than the actually observed first-order phase transition at T_c.

5. Discussion and comparison with experiment

In order to give a visual impression, the analytic behaviour of the correlation function $\langle Q_1 Q_1\rangle_\omega$, determining the neutron scattering cross sections, has been plotted in figures

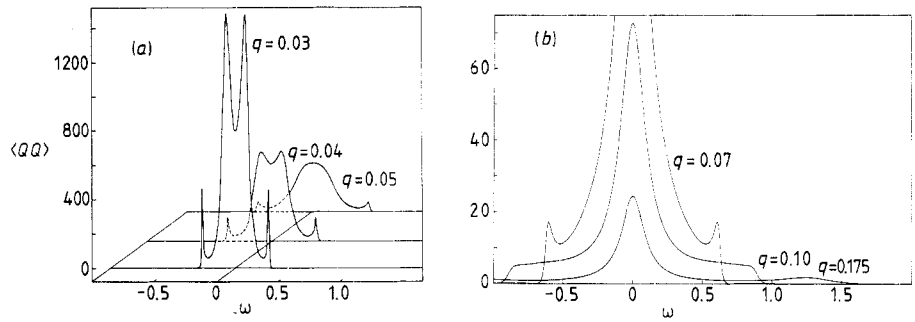

Figure 10. Phonon correlation function (66) for $q = (q_x, 0, 0)$: (*a*) for small $q = q_x$ such that softened modes appear; (*b*) for larger q, where at $q = 0.175$ the phonon peak is well separated from the central line. For smaller q the c_{44} mode merges with the central mode and 'c_{66} ghosts' appear, not (yet) resolved in neutron scattering.

10(*a*) and (*b*) for $\boldsymbol{q} = (q_x, 0, 0)$ and $\omega_1(q_x)$ in the interesting range from $\omega_1(q_x) < 6\gamma kT$ to $\omega_1(q_x) \geqslant 6\ \gamma kT$; softening and overdamping of $\omega_1(q_x)$ are readily visible, and at the same time peaked structures, caused by the other modes, may appear. The influence of $\omega_3^2 \sim c_{11}$ is not really discernible since c_{11} ($\simeq 6c_{44}$) is so much larger than even its softened version ω_{3s} gives relatively too little intensity; so figure 10 mostly reflects the behaviour of $\omega_1^2 \sim c_{44}$ and $\omega_2^2 \sim c_{66}$. The narrow peaks below $q_x = 0.07$ have not been resolved experimentally. Figure 11 shows what is to be expected (and is found) as intensity from the inelastic scattering experiments near $\boldsymbol{K} = (0, 0, 2)$ and $\boldsymbol{q} = (q_x, 0, 0)$ (details in Graf *et al* 1989), taking into account the experimental resolution. For figures 10 and 11, the parameters resulting from fitting the experimental data have been used. The experiments could not be extended to the small q of figure 10(*a*). The $CsCuCl_3$ crystals are very sensitive to heating and cooling across T_c: they apparently develop micro-cracks, and Bragg tails and powder lines appear excluding the small-q range from reliable observation. Further experiments are planned on a new crystal heated just once to $T > T_c$.

The theory contains the five elastic constants, the dipole strength and γkT, the inverse average time a spin stays in one state. For the elastic constants the room-temperature values from Soboleva *et al* (1976) can be used as starting values, except for c_{33} and c_{44} for which from Lüthi's (1977) data high-temperature values can be extrapolated. The dipole strength, that is the factor $Vc_{44}\Delta d/d$ or $Vc_{66}\Delta d/d\sqrt{2}$ in (12), can be estimated by relating it to the Jahn–Teller energy. The parameter γkT is unknown, and if enough data are available (elastic and inelastic) to give a reasonable set of elastic constants and dipole strength, γkT can be considered 'measured' by this experiment. The observed overdamping has already shown that neutron scattering has the right intrinsic timescale for the 'spin-flip rate' and can cover the range from 'almost static' to 'dynamic' Jahn–Teller effect.

For an estimate of the softened modes or elastic constants expected in ultrasound experiments the quantities h_i^2/T, from (67), are important. With (16) and (51) and $\boldsymbol{q} = (q_x, 0, 0)$ one finds

$$\begin{aligned} h_1^2(q_x)/T &= Ac_{44}\omega_1^2 \\ h_2^2(q_x)/T &= Ac_{66}\omega_2^2/2 \\ h_3^2(q_x)/T &= Ac_{66}^2\omega_3^2/2c_{11} \end{aligned} \tag{75}$$

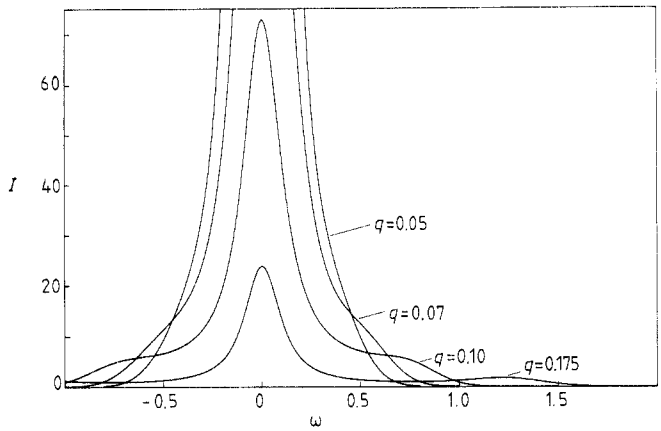

Figure 11. Inelastic neutron scattering intensity with $q = (q_x, 0, 0)$ near $K = (0, 0, 2)$: theory (80) folded with the instrumental resolution (3 meV) (details in Graf *et al* 1989).

where $A = \rho v^2/mkT$, $v = V\Delta d/d$. With ω_1^2 from (52), q_x in reciprocal-lattice units with $2\pi/a^* = 4\pi/a\sqrt{3} = 1.003$ Å^{-1}, and for $\boldsymbol{q} = (0, 0, q_z)$, q_z in units of $2\pi/c^* = 1.01$ Å^{-1}:

$$h_2^2(q_z)/\bar{T} = h_3^2(q_z)/\bar{T} = Ac_{44}\omega_1^2 \qquad \omega_2^2 = \omega_3^2 = c_{44}q_z^2/\rho \tag{76}$$

$$h_1^2(q_z) \sim \sum_r |P_{zz}^r|^2 = 0 \qquad \omega_1^2 = c_{33}q_z^2/\rho. \tag{77}$$

The reason why ω_1 is not softened can be traced to the model for the direction of the stretched octahedra in space (figure 4(*a*)), which keeps the trigonal symmetry around the z axis: as the JT distortions change direction, 'nothing happens' along c, that is all $P_{zz}^r = 0$. In fact Lüthi's (1977) measurements of c_{33} (longitudinal mode along c) shows no softening above T_c but a rise of c_{33} at T_c of about 10%.

Since the elastic constants and the other parameters as theoretically expected and found experimentally are discussed in the accompanying paper by Graf *et al* (1989), we only note the results for the softening elastic constants to be expected (but not observable by neutrons in the accessible $\boldsymbol{q}$-range). The 'bare' values ($T \gg T_c$) were found to be

$$\begin{aligned} \omega_1^2 &\sim c_{44} = 4.23 \times 10^{10} \text{ erg cm}^{-3} \\ \omega_2^2 &\sim c_{66} = 8.2 \times 10^{10} \text{ erg cm}^{-3} \\ \omega_3^2 &\sim c_{11} = 29 \times 10^{10} \text{ erg cm}^{-3} \end{aligned} \tag{78}$$

and $A = 0.093 \times 10^{-10}$ cm^3 erg^{-1}. These values go into the calculation of the softened modes (peaks of (66) at $\omega_i \ll \gamma kT$):

$$\begin{aligned} \omega_{S1}^2 &= (q_x^2/\rho)\, 0.76 \times 10^{10} \\ \omega_{S2}^2 &= (q_x^2/\rho)\, 6.4 \times 10^{10} \\ \omega_{S3}^2 &= (q_x^2/\rho)\, 26.8 \times 10^{10}. \end{aligned} \tag{79}$$

all in cgs units. Obviously, c_{44} becomes anomalously small, as had been noticed by Lüthi in ultrasound velocity measurements.

One can also calculate the fictitious second-order transition temperature (73): $T_0 = 382$ K for $\boldsymbol{q} = (q_x, 0, 0)$ while $T_c = 423$ K.

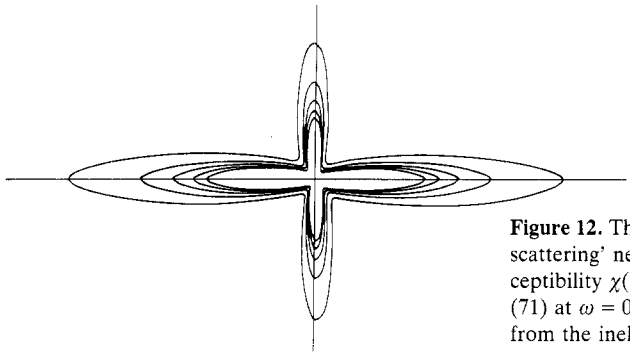

Figure 12. Theoretical predictions for 'dense Huang scattering' near $\boldsymbol{K} = (2,0,1)$ corrected with the susceptibility $\chi(q, T = 428\,\mathrm{K})$. Iso-intensity lines from (71) at $\omega = 0$ are plotted using the elastic constants from the inelastic data fits.

At 428 K the linewidth of the central peak is

$$\Gamma_{\text{centre}} = 6\gamma kT(1 - T_0/T) = 0.86(1 - 373/428) = 0.1\,\text{meV}. \tag{80}$$

The experimental result for 428 K is $6\gamma kT = 0.86$ meV. Γ_{centre} is about 50% of the resolution.

The central line would yield a quasi-elastic picture of the Jahn–Teller distortions, were it not for the shoulders from the broadened phonons. Therefore quasi-elastic scattering will pick up phonon contributions, broadening the 'waists' of the Huang patterns (figures 12 and 13). Theoretical predictions of the Huang pictures have to be calculated by integration of the dynamical scattering cross section folded with the resolution around $\omega = 0$.

The interpretation of $6\gamma kT = \Gamma(T)$ involves the energy surface of the Jahn–Teller distorted states, the 'Mexican hat' with its three minima with the 'warping energy' β impeding transitions between them. We expect an Arrhenius law

$$\Gamma(T) = 6\gamma_0 kT\,\mathrm{e}^{-2\beta/kT} \tag{81}$$

to hold. From three measured values for $\Gamma(T)$ from inelastic data (Graf *et al* 1989) $2\beta =$ 450 K gives a good fit. This is somewhat lower than the usually given free cluster values of 200 cm^{-1} for β, but this tendency is expected in the compound (Deeth and Hitchman 1986).

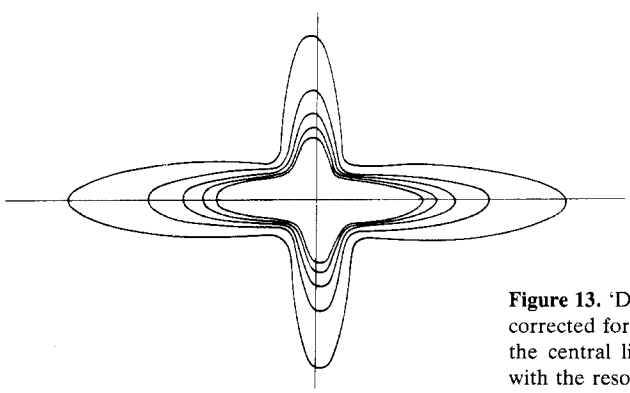

Figure 13. 'Dense Huang scattering' as in figure 12, corrected for phonon contributions in the wings of the central line, based on integrating (70) folded with the resolution.

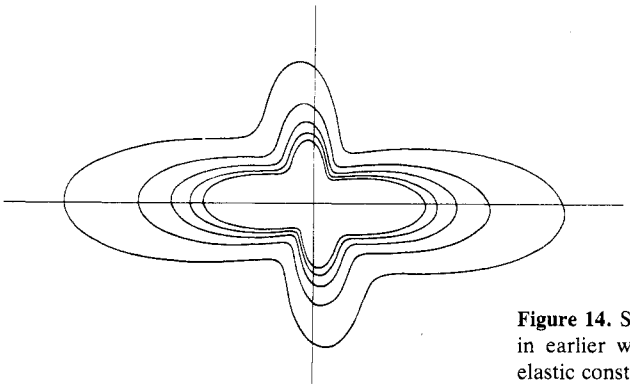

Figure 14. Static 'dense Huang scattering', (82), as in earlier work (Schotte 1987) but with the new elastic constants, near $\boldsymbol{K} = (2,0,1)$.

Finally we discuss our new understanding of 'dense Huang scattering' as it represents itself in the small-ω limit of the dynamical description. Earlier we had derived the static expression (Schotte 1987)

$$\mathrm{d}\sigma/\mathrm{d}\Omega = \bar{b}^2 \tfrac{1}{6} \sum_r |\boldsymbol{Q} \cdot \mathbf{D}^{-1} P^r \boldsymbol{q}|^2. \tag{82}$$

It is now corrected in two ways.

A major modification is due to the T- and $\boldsymbol{q}$-dependent susceptibility $\chi(\boldsymbol{q})$ read off from (72). $T_0(\boldsymbol{q})$ from (73) and therefore $\chi(\boldsymbol{q})$ do not depend on the modulus of $\boldsymbol{q}$ but on its direction. Therefore the typical Huang behaviour of the intensity as q^{-2} is not changed.

Qualitatively the shape of the iso-intensity lines becomes slimmer and more symmetric (figures 12 and 15). This shape is then widened in the middle by the phonon and resolution effects mentioned (figure 13). This is much closer to the experimental findings (see Graf *et al* 1989) than the naive Huang picture of (82) in figure 14.

The fact that the transition temperature depends on the q direction points to competing order parameters, which necessitates a further mechanism to trigger the first-order transition at $T_c > T_0$. As discussed by Graf *et al* (1989), (72) taken literally leads to an iso-intensity contour near (2,0,1) with lobes more extended along x^* than observed. Perhaps one sees a true precursor of the first-order transition.

6. Summary and conclusions

We have described the high-temperature phase of the $ABCl_3$ (A = Cs, Rb; B = Cu, Cr) compounds as a lattice of elastic dipoles corresponding to the JT stretched octahedra of the Cl^- cage around Cu or Cr, and calculated the consequences for inelastic and quasi-elastic neutron scattering, assuming no other dynamics than a flip rate for the corresponding pseudo-spins.

This description was initiated by the observation that interesting phenomena for $q \to 0$ (ultrasound, Huang scattering) had been found for $CsCuCl_3$. This was followed by inelastic neutron scattering experiments described in a separate paper (Graf *et al* 1989).

As a result, a set of elastic constants and predictions of their softening behaviour towards a second-order phase transition some 50 K below the observed first-order

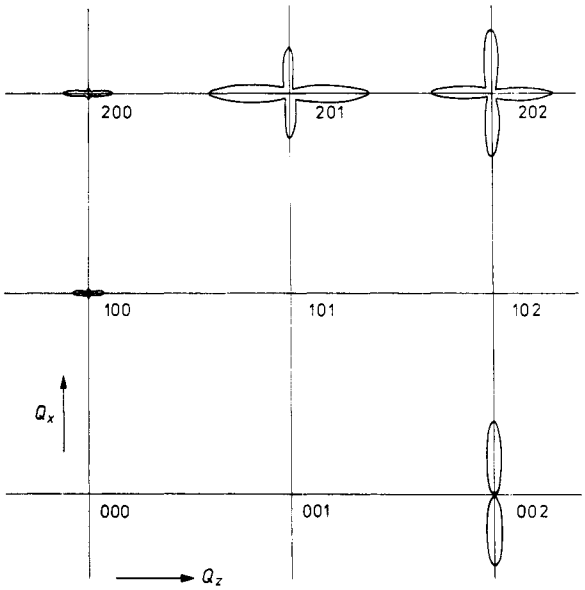

Figure 15. Diffuse scattering iso-contours in the x^*z^* scattering plane to be expected in the high-temperature phase close to T_c for $CsCuCl_3$ calculated as for figure 12.

transition have been found. Also a spin-flip rate was deduced which is supposed to be related to the warping energy of the JT complex overcome by the thermal activation; this is the only place where optical phonons come into play.

The model also allows the calculation of the pseudo-spin interactions. We found repulsive interactions between distortive states along c which prevent the long octahedron axes from meeting at the same anion. In the hexagonal plane, the sign of the interaction depends on the direction of the vector connecting the partners. Thus rows of ferrodistortively ordered distortions of one type alternating with such rows of a different distortive type can be favourable but, depending on elastic constants, purely ferrodistortive arrangements are also possible. Thus the intermediate structures of the Rb compounds (where the cell is not yet enlarged along c) are immediately plausible together with the predicted softening of the c_{44} shear mode (monoclinic angle of $RbCrCl_3$) and the c_{66} shear mode (orthorhombic distortion of $RbCuCl_3$). Some of these structural characteristics have already been discussed by Crama (1980) and Crama and Maaskant (1983). We could add predictions about the sign and relative size of the interactions within the elastic dipole model. There is still room to try out theoretical predictions of the anisotropic Potts model; there seem, however, to be none available for the hexagonal system and three interaction parameters (two in the plane and one along c).

We have excluded from consideration the mechanism for the first-order phase transition for which experimentally no precursor effect could be observed.

In the future more detailed knowledge of the behaviour of c_{33} is sought. When we know better what happens along c, we will try to find connections to recent considerations about the first-order transition of $CsCuCl_3$ by Maaskant and Haije (1986). Since we seem to have found a way to determine experimentally the warping term, it will be interesting to extend it to other compounds with a different JT ion (Cr^{2+}) and/or different elastic environment (Rb^+).

Acknowledgments

The authors greatly profited from discussions with M A Hitchman, K Michel, N Pyka, D Reinen, K D Schotte, G Shirane, H Thomas, H Trinkaus and Y Yamada.

References

Crama W J 1980 *Thesis* University of Leiden, The Netherlands
Crama W J and Maaskant W J A 1983 *Physica* B **121** 219
Deeth R J and Hitchman M A 1986 *Inorg. Chem.* **25** 1225
de Fontaine D 1979 *Solid State Phys.* **34** 73
de Raedt B, Binder K and Michel K H 1981 *J. Chem. Phys.* **75** 2977
Friedman Z and Felsteiner J 1974 *Phys. Rev.* B **9** 337
Graf H A, Shirane G, Schotte U, Dachs H, Pyka N and Iizumi M 1989 *J. Phys.: Condens. Matter* **1** 3743
Graf H A, Tanaka H, Dachs H, Pyka N, Schotte U and Shirane G 1986 *Solid State Commun.* **57** 469
Höck K-H, Schröder G and Thomas H 1978 *Z. Phys.* B **30** 403
Khatchaturian A G 1965 *Sov. Phys.–Crystallogr.* **10** 248
—— 1966 *Sov. Phys.–Crystallogr.* **10** 383
Landau L D and Lifshitz E M 1965 *Lehrbuch der Theoretischen Physik* (Berlin: Springer) vol V, p 415ff and vol VII, p 33
Lüthi B 1977 in Hirotsu S J 1977 *J. Phys. C: Solid State Phys.* **10** 967 and private communication
Maaskant W J A and Haije W G 1986 *J. Phys. C: Solid State Phys.* **19** 5267
Mori M, Noda Y and Yamada Y 1980 *J. Phys. Soc. Japan* **48** 1288
Reinen D and Friębel C 1979 *Structure and Bonding* vol 37 (Berlin: Springer)
Samukhin A N 1982 *Sov. Phys.–Solid State* **24** 1297
Schotte U 1987 *Z. Phys.* B **66** 91
Schröder G and Thomas H 1976 *Z. Phys.* B **25** 369
Soboleva L U, Sil'vestrova J M, Perekalina Z B, Gil'varg A B and Martyshev Y N 1976 *Sov. Phys.–Crystallogr.* **21** 660
Tanaka H, Dachs H, Iio K and Nagata K 1986a *J. Phys. C: Solid State Phys.* **19** 4861
—— 1986b *J. Phys. C: Solid State Phys.* **19** 4879
Terauchi H, Mori M and Yamada Y 1972 *J. Phys. Soc. Japan* **32** 1049
Yamada Y, Takatera H and Huber D L 1974 *J. Phys. Soc. Japan* **36** 641